Journal of Power Sources, *16* (1985) 141 - 168

A STUDY OF THE PHASE COMPOSITION, CRYSTALLINITY, MORPHOLOGY, POROSITY AND SURFACE AREA OF LEADY OXIDES USED IN LEAD/ACID BATTERY PLATES

G. L. CORINO*, R. J. HILL, A. M. JESSEL, D. A. J. RAND and J. A. WUNDERLICH

CSIRO, Institute of Energy and Earth Resources, Division of Mineral Chemistry, P.O. Box 124, Port Melbourne, Vic. 3207 (Australia)

(Received September 10, 1985)

Summary

X-ray diffraction, differential scanning calorimetry and wet-chemical techniques have been used for the quantitative phase analysis of leady oxides prepared by both the Barton pot and the ball mill processes and obtained from a world-wide selection of lead/acid battery and lead oxide manufacturers. Results indicate that large differences in composition, crystallinity, particle size, morphology, surface area and pore-size distribution exist both within and between the products obtained from the two processes. In general, ball mill oxides have smaller particles, are less crystalline, have a lower β-PbO content, have a higher content of free lead, and higher surface areas than oxides produced by the Barton pot method. Optical microscopy and porosimetry measurements reveal significant differences in the morphology and pore-size distributions of the oxides that are consistent with the phase analysis results. Storage of both types of oxide for even short periods of time at room temperature results in a significant conversion of the free lead and non-crystalline material to α-PbO. Such variations in the chemistry and the morphology of leady oxide are expected to influence the physicochemical characteristics of the pasted, cured and formed active material in lead/acid plates, as well as the subsequent performance of these plates under charge/discharge cycling service.

Introduction

The basic starting material for lead/acid battery plates is generally referred to as "leady" or "grey" oxide. Commercial leady oxide usually contains 65 - 83 wt.% of lead monoxide (PbO) and 17 - 35 wt.% of finely divided lead [1, 2]. This oxide is the main ingredient of the pastes used

*Now at Australian National Animal Health Laboratory, P.O. Bag 24, Geelong 3220, Australia.

0378-7753/85/$3.30

for flat positive and negative plates, but it is blended with up to 50 wt.% red lead (Pb_3O_4) when material is prepared for tubular positive plates. There are two basic methods for manufacturing leady oxide, the Barton pot process (brand names: Balox, Chloride, Hammond, Linklater, Minimet) and the ball mill process (brand names: Chloride, Hardinge, Heubach, Shimadzu, Tudor).

In the Barton pot process for making this material, molten lead is oxidized by air at a specified temperature (330 - 400 °C) in a reaction pot. Usually, a spray of molten lead droplets is fed into the reaction pot and any accumulated bulk molten metal is broken up again into droplets by a revolving paddle that forces the lead against a fixed baffle arrangement inside the pot. Sometimes, the lead is melted directly in the reaction pot itself. In both procedures, a stream of air, blown over the molten droplets, oxidizes the lead and, once this reaction is in progress, the temperature is maintained by the oxidation itself. The resulting oxide powder is carried by the air stream into a size classification apparatus where the specified particle-size range is separated out and the coarser material is returned to the pot. By careful control of the pot temperature, the paddle rotation speed, the rate of air flow, and the size of the operating load (determined by the rate of solid or molten lead feed), battery oxide of the desired chemical composition can be obtained. Generally, the particle-size distribution of the resulting oxide is satisfactory for good reaction with sulphuric acid in the paste-mixing process (*i.e.* a high acid-absorption value). However, in order to avoid pasting and plate-making difficulties, some battery manufacturers pass the Barton pot oxide through a hammer mill to produce finer particles with greater reactivity.

Alternatively, leady oxide may be prepared in a ball mill process. Here, lead balls, cylinders, or entire lead ingots are tumbled in a steel drum that is rotated with its central axis in the horizontal plane. The heat generated by the friction between the lead pieces is sufficient to start oxide formation in the presence of an air stream blown through the drum. This, in turn, generates more heat and the particles of lead that are rubbed off by the abrasion are converted to leady oxide of the required chemical composition. Cooling the drum with air or water prevents excessive heating. The oxide is removed by discharge through small holes in the periphery of the drum (*e.g.* Tudor mills, operated at 70 - 90 °C), or by entrainment in an air stream passed through a cylindrical drum (*e.g.* Shimadzu mill), or by overflowing at a cone-shaped exit that is fitted with screens (*e.g.* Hardinge mill, operated at 160 - 190 °C). The air-sweep principle is now applied also to Hardinge mills, and both these and Shimadzu mills are usually fitted with cyclone classifiers. Oxide of consistent quality can be obtained through careful control of the residence time of the material in the mill. In the Shimadzu and Hardinge mills, this is achieved by adjusting both the flow rate and the temperature of the air stream, the mill speed, the mill charge temperature, and the amount of mill charge. More detailed accounts of leady oxide production methods are given in refs. 2 - 4.

The advantages and characteristics variously claimed for the Barton pot process (without subsequent grinding) and the ball mill process are given in Table 1. Often, these are bold statements in the literature with little or no supporting experimental data; we are not aware of any detailed comparison of the two oxide production methods. In summary, the Barton pot process is considered to be more economical (*i.e.* has less energy demand) and to give an oxide that is easier to handle, whereas the ball mill method produces an oxide that has smaller particles with greater chemical reactivity during pasting (*i.e.* a higher acid-absorption capability) and, subsequently, a formed active material with higher initial electrical capacity. However, after a short period of service in batteries, differences in the performance of plates prepared by using either of the two types of oxide are generally considered by battery manufacturers to be negligible, given that the process variables of the oxide production are optimum. As will be seen below, we question such a sweeping generalization — one that is made irrespective of the type or service of the battery.

The leady oxide produced by both of the above processes generally consists of a mixture of lead particles with both modifications of lead monoxide, and possibly with a small proportion of Pb_3O_4 (red lead or min-

TABLE 1

Comparison of Barton pot (unground) and ball mill processes for leady oxide production

Parameter	Barton pot	Ball mill
Economics	Initial cost lower	—
	Most energy efficient	—
Operation	Oxide easier to handle, less prone to aggregation	Higher production rate per weight (more lead under process)
	Process easier to control	
	Higher production rate per unit space	
	Higher conversion of lead to lead oxide	
Oxide	Oxide and lead particles more equidimensional	Lead particles flatter and thinner
	Greater apparent bulk density	Oxide particles smaller (lower median particle diameter) and more reactive
	Higher β-PbO content	
	Longer shelf life	
		Higher free-lead content
Paste	Paste mixing and pasting easier	Higher acid absorption
		Better paste consistency at very low densities
Plate characteristics		
Curing	—	Process faster
		Stronger active material
Formation	—	Greater surface area
		Higher initial capacity

ium). The lead monoxide occurs as a red form, known as α-PbO (litharge) that has a tetragonal crystal structure, and as a yellow form known as β-PbO (massicot) with an orthorhombic structure. The transition temperature of α-PbO to β-PbO is around 480 °C (the actual temperature depends markedly on the oxide preparation history [3]). The internal temperature of a ball mill is well below this temperature, but this may not be the situation with the Barton pot process. Thus, whereas ball mill leady oxide usually contains very little β-PbO, a significant quantity of this monoxide can be present in the Barton pot material.

The relative proportion of the two polymorphs of PbO is important in the production of battery plates since reports have claimed [5, 6 and references therein] that it gives rise to different basic lead sulphate phases during the curing process: α-PbO produces tribasic lead sulphate ($3PbO \cdot PbSO_4 \cdot H_2O$), while β-PbO gives tetrabasic lead sulphate ($4PbO \cdot PbSO_4$). These sulphate phases, in turn, produce different plate performance characteristics during charge/discharge cycling. Since it is generally agreed [7] that α-PbO is the preferred starting phase for the paste-making process, particularly for flat positive plates, the operating conditions for the Barton pot must be carefully controlled to ensure that the bulk of the oxide is in this form. Thus, quantitative determination of oxide composition is a necessary prerequisite to the satisfactory control of the oxide manufacturing process.

Earlier studies of the phase composition of leady oxides [5, 8, 9] have attempted to develop a routine X-ray diffraction (XRD) method for monitoring changes in oxide composition but have suffered from one or more of the following limitations: (i) no estimate has been made of the Pb_3O_4 content of the leady oxide; (ii) all analyses have been normalized to 100 wt.%, *i.e.* no estimate has been obtained for the content of non-crystalline or amorphous* material; (iii) the free-lead content has been determined by unrefined wet-chemical or XRD methods; (iv) the X-ray calibration constants have been determined by experiment from "standard" materials of uncertain crystallinity and purity; (v) the amount of each phase has been estimated from the intensity of (at most) only two diffraction peaks; and (vi) few (if any) studies have been undertaken on commercially produced leady oxides.

In this work, we describe methods for the accurate determination of the phase composition of leady oxides that address all of the above experimental limitations of earlier work. In addition, we present the results of studies on the composition, crystallinity, morphology, porosity and surface area of oxide samples obtained from both ball mill and Barton pot commercial processes, and from a variety of manufacturers.

*The term "amorphous" is used here to refer to material that does not give rise to normal XRD peaks because: (i) it is truly structureless; (ii) it has a very small crystallite size (*i.e.* only about 100 Å or less); or (iii) it contains a very large concentration of crystal defects.

Experimental

Phase analytical procedure

As indicated above, the two most commonly used methods of leady oxide production involve the oxidation of metallic lead either from the molten state (Barton pot) or from the solid state by rolling and grinding (ball mill). The product of both processes is an intimate mixture of α-PbO, β-PbO, Pb_3O_4 and metallic lead. As will be seen below, these phases do not always occur as discrete particles. For example, some of the lead particles are only partially oxidized and are present as a metallic core within the oxide product; further, PbO particles may be contained within Pb_3O_4 particles as the oxidation proceeds. Encapsulation of lead causes hitherto unrecognized problems in the experimental determination of its abundance in the mixture when using an XRD phase analysis technique: the oxide coating strongly absorbs X-rays and, therefore, selectively diminishes the magnitudes of the beams both incident to, and diffracted from, the lead particles. Furthermore, small lead particles have a large surface-area/mass ratio and consequently have a high chemical reactivity. Thus, the more commonly used "in factory" wet-chemical methods of lead determination that rely on the selective dissolution of the oxides can result in the removal of some of the more finely divided lead particles, thereby producing an underestimate of the total lead content of the sample.

We have avoided these problems by using the technique of differential scanning calorimetry (DSC) to determine the free-lead content of the oxide samples prior to XRD and/or wet-chemical analysis. The DSC technique is able to measure the lead content independently of its particle size, shape, or degree of encapsulation by the oxides. The method measures the heat of melting of the lead particles in a given oxide sample and compares this with the enthalpy of fusion of an equivalent mass of pure lead. The amount of non-crystalline, or amorphous, material in the sample is calculated by the difference from 100 wt.% using the DSC estimate of the lead content in conjunction with the XRD-determined lead oxide content. In the absence of a DSC determination, the free-lead content is estimated by a refinement of the more generally used acetic acid dissolution method.

Differential scanning calorimetry

Differential scanning calorimetric (DSC) measurements were carried out using a SETARAM DSC III instrument (for a description of this equipment and its functions see Ref. 10). Heat flow data were collected on a Hewlett Packard 3421A Data Acquisition and Control Unit, and processed by a Hewlett Packard 85 microcomputer.

The DSC instrument was supplied with a "Joule effect" cell that was equipped with an electrical resistance heater controlled by an adjustable power supply. Calibration was achieved by placing the cell in the detection zone and measuring the enthalpy of fusion of 10 to 50 mg samples of high purity lead (Koch Light 99.9999%). The observed enthalpy of fusion was

-22.77 ± 0.05 J g^{-1} and the melting point was 327.3 ± 0.1 °C. The corresponding critically assessed [11] values are -23.16 ± 0.02 J g^{-1} and 327.4 °C, respectively. Comparison of these values with those observed experimentally demonstrates that the DSC calibration was accurate to within ±1%. The enthalpy value used to calculate the lead contents was -22.77 J g^{-1}. For measurements of the free-lead content of the leady oxides, the samples were weighed into open alumina micro-boats and heated under a stream of argon (5 ml min^{-1}). The DSC instrument was programmed to heat a sample quickly to 322 °C, then at 1 °C min^{-1} to 342 °C.

Plots of the DSC heat flow as a function of sample temperature for pure lead and three leady oxides are shown in Figs. 1(a) - (d). The size of the DSC peak varies directly with the amount of metallic lead in the samples, that is, with the weight of sample used (about 50 mg in the case of the pure lead in part (a) and about 100 mg for the oxide samples in parts (b) - (d)) and the weight fraction of lead in the sample (100, 14, 11 and 39 wt.% in parts (a) - (d), respectively). It can also be seen that the shape of the DSC peak obtained from pure lead is markedly different from that observed for the leady oxides. This is due to the different thermal responses of the oxides present in the latter samples. Moreover, the DSC peak profile varies considerably between the different oxides, reflecting differences in the shape, size and degree of encapsulation (and chemical reactivity) of the lead particles in these samples. However, the melting point of the lead varies by less than 0.5 °C between the four samples, and this demonstrates the reliability of the DSC method for free-lead determinations.

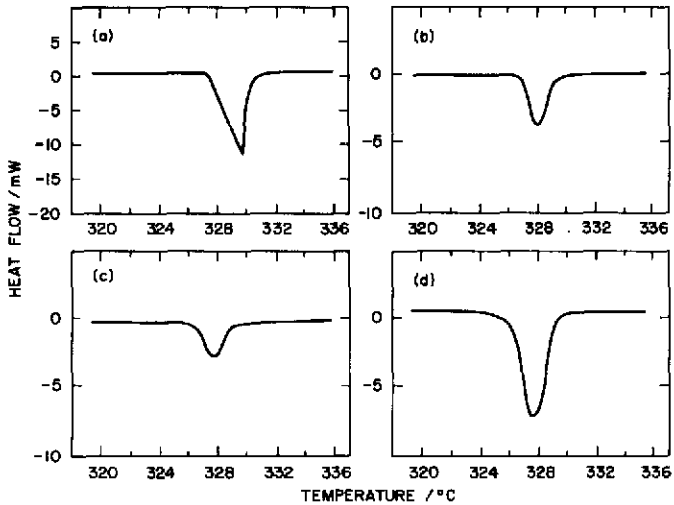

Fig. 1. Variation of heat flow with temperature in the vicinity of the melting point of lead in samples of (a) Koch Light 99.9999% Pb, (b) Australian Barton pot oxide (BP16 in Table 3) (14.4 wt.% Pb), (c) New Zealand Barton pot oxide BP17 (10.7 wt.% Pb), and (d) U.K. ball mill oxide BM4 (38.6 wt.% Pb).

Dissolution with acetic acid

Experimental conditions for the determination of the free-lead content of leady oxides by the well-known acetic acid method [12] were optimized by conducting tests on pure lead and on leady oxide samples of known (DSC) free-lead content. The following procedure was finally selected and is a refinement of various methods quoted in the literature [13 - 15]. A mixture of 2 ml of glacial acetic acid, 20 ml of 15 wt.% ammonium acetate and 0.3 g of ascorbic acid was made up to a volume of 125 ml with distilled water and heated to a temperature of 75 - 80 °C. The hot liquid was poured into a flask containing 3 g of the oxide sample and the solution was stirred with gentle heating. The coagulated lead residue was recovered by filtration, dried under nitrogen, and weighed. Comparison of the acetic acid (HAc) determinations with the results of DSC measurements carried out on the same samples indicates that the acetic acid method is accurate to within ±2 wt.% lead (see Fig. 3(a) and Table 3 below).

X-ray powder diffraction

X-ray powder diffraction analysis is the most commonly used method for determining the relative abundances of crystalline compounds in multi-phase mixtures. Accurate XRD determination of phase abundance is, however, not a trivial task since the diffraction-peak intensities from a particular phase are not, in the general case, a simple linear function of the concentration of the phase and, furthermore, the peak intensities cannot be related to those of another phase without extensive, and often laborious, calibration [16]. In addition, phase analysis of the lead oxide system is particularly difficult because of problems arising from: (i) severe diffraction-peak overlap; (ii) high absorption coefficients; and (iii) uncertainties in the degree of preferred orientation, crystallinity, stoichiometry and variability of particle size [5, 8, 9, 17 - 20, and references therein].

The XRD method selected here for the analysis of leady oxide is a version of the internal-standard technique previously developed in our laboratory for the study of formed positive plates [21, 22]. This technique was specifically chosen because it is more accurate than other XRD procedures and because it allows determination of the amount of both crystalline and amorphous material in the sample.

The fundamental equation relating phase concentration W and diffracted peak intensity I in the internal-standard method is

$$W_i = \frac{I_i}{I_s} \frac{W_s}{\mathrm{RI}_i} \tag{1}$$

where RI_i, the so-called "reference intensity ratio", is a constant for a given phase i in the presence of a standard phase s added in the weight proportion W_s. The weight fraction W_i of the phase i is obtained by measuring the diffracted peak intensity ratio I_i/I_s for known values of W_s and RI_i. Ceric oxide (CeO_2) was selected as the internal-standard material and was fired at 1200 °C for 24 h to decrease the diffraction peak width and to ensure stoichiometry.

For the reasons outlined previously [18 - 20], the values of RI_i were obtained not by experimental calibration, but by calculation from first principles using the known crystal structure and X-ray scattering properties of the individual phases. That is, from the expression

$$RI_i = \frac{Q_i}{Q_s} \frac{D_s}{D_i} \tag{2}$$

where Q is the calculated powder diffraction intensity, and D is the product of the unit-cell volume and the mass of the unit-cell contents (in atomic mass units) for each phase. The unit-cell dimensions and atomic positional and thermal vibrational parameter values necessary for the calculation of Q and D for each of the phases α-PbO, β-PbO, Pb_3O_4 and Pb were obtained from the literature [18, 19, 21, and references therein].

In order to minimize the effects of preferred orientation and peak overlap in the α-PbO and β-PbO components, the intensity of three separate reflections was measured for both of these phases. Similarly, the above-mentioned problems with lead encapsulation by oxide required that three peaks from the lead phase also be measured. However, for the Pb_3O_4 and the internal-standard CeO_2, only one (intense) reflection was measured. After an extensive series of trials, the diffraction record between 25.0° and 55.4° 2θ was selected and divided up into a total of eleven discrete scanning regions for the phase analysis procedure (see Fig. 2(a) below).

Table 2 gives numerical details of the scanned regions, together with the calculated and observed values of the peak intensities for several "standard" samples. Simulated powder diffraction patterns for 1:1 mixtures (by weight) of each of the phases with CeO_2 over the range scanned in the phase analysis procedure are given in Figs. 2(a) - (d). These patterns simulate the phase analysis record obtained from a standard X-ray diffractometer using nickel-filtered Cu Kα radiation: the peaks have a full width at half-maximum of 0.17°, and an intermediate Lorentzian peak shape. The upper and lower rows of vertical lines immediately below each pattern represent the positions of all possible Bragg reflections allowed by the space-group symmetry of the first- and second-mentioned phase in each pattern, respectively. The three small rectangular areas below the pattern in Fig. 2(a) are the regions selected for background determination.

Oxide samples were dried for 2 h at 120 °C prior to analysis. For each sample, approximately 0.6 g of the material was added to about 0.3 g of CeO_2 (with exact weights recorded for use in the later data analysis) and the resulting mixture was ground for 3 min in a Retsch-type MM2 mixer/mill. This grinding time was selected as a compromise between the desire to produce a reduction in particle size together with an increase in phase homogeneity of the samples, without causing a significant conversion of β-PbO to α-PbO. The sample was then back-pressed into an aluminium holder and the surface scraped flat with a straight edge. The holder was mounted in a Philips PW1050 diffractometer equipped with an autoscanner attachment. Integrated X-ray intensities were collected over the eleven scan

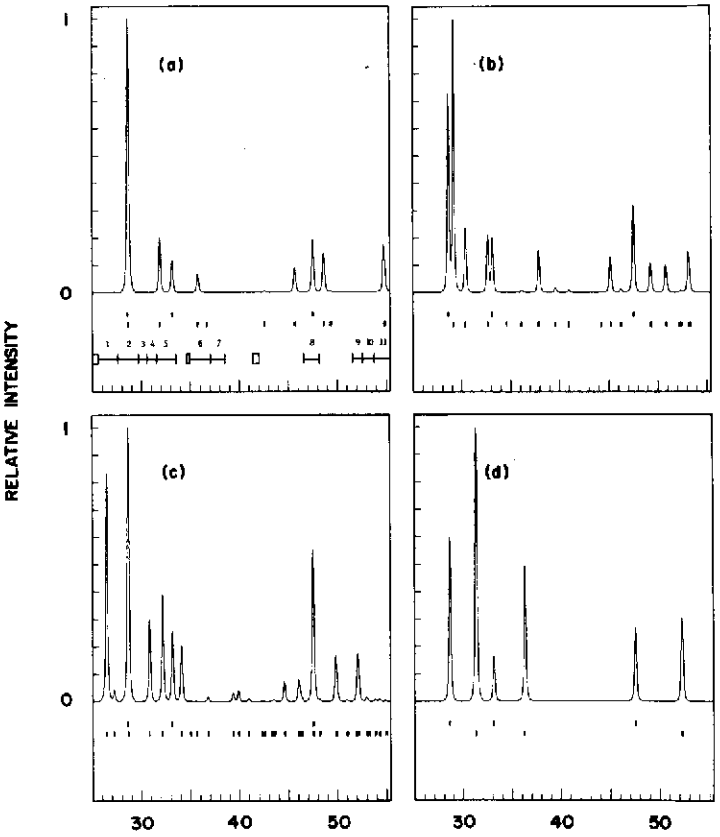

Fig. 2. Simulated Cu Kα XRD patterns for 1:1 (by weight) mixtures of CeO_2 with (a) α-PbO, (b) β-PbO, (c) Pb_3O_4, and (d) Pb. In (a) the eleven ranges of 2θ scanned for the intensity measurements are indicated by number, along with the three regions used for background determination. The two rows of vertical lines immediately below each pattern represent the positions of all possible Bragg peaks from the two components in the mixture.

ranges described above using a step width of 0.01° 2θ, and a step counting time of 0.4 s; these settings correspond to a continuous scanning rate of 1.5° min^{-1} and an analysis time of about 40 min per sample. The data were punched on to paper tape for subsequent computer analysis.

For mixtures of all five compounds (namely α-PbO, β-PbO, Pb_3O_4, Pb and CeO_2), only three of the eleven scan regions (numbers 1, 3 and 7 in Table 2 and Fig. 2) contain peaks from a single phase (β-PbO or Pb_3O_4). These free-standing peaks were used at the start of the phase analysis procedure (after the subtraction of background) to define the amounts of Pb_3O_4 and β-PbO present. Using the known relative intensities of the peaks from these two phases in the other eight scan regions, the peak intensities for the remaining phases were then determined by peak "stripping". When the free-lead content of the sample had been previously determined by

TABLE 2

Diffraction-peak Miller indices and their calculated and observed relative intensities for the 2θ ranges scanned during the phase analysis procedure

Scan No.	2θ range (deg)	CeO_2[a]			α-PbO[b]			β-PbO[b]			Pb_3O_4[b]			Pb[c]		
		(*hkl*)	I_{calc}	I_{obs}	(*hkl*)	I_{calc}	I_{obs}	(*hkl*)	I_{calc}	I_{obs}	(*hkl*)	I_{calc}	I_{obs}	(*hkl*)	I_{calc}	I_{obs}
1	25.61 - 27.60		—			—			—		(121) (002)	100.0	100.0		—	
2	27.61 - 29.70	(111)	100.0	100.0	(011)	100.0	100.0	(111)	100.0	100.0	(220)	12.50	17.6		—	
3	29.71 - 30.57		—			—		(200)	24.58	34.5		—			—	
4	30.58 - 31.55		—			—			—		(112)	36.00	34.3	(111)	100.0	100.0
5	31.56 - 33.40	(002)	28.57	29.5	(110)	31.62	28.0	(020)	22.14	21.4	(130)	46.37	47.6		—	
6	34.90 - 37.00		—		(002) (111)	11.28	13.0	(120)	0.70	2.5	(131) (122) (230)	2.60	1.7	(002)	50.32	55.1
7	37.01 - 38.50		—			—		(002) (021)	16.68	14.1		—			—	
8	46.70 - 48.10	(022)	52.28	56.2		—			—		(123)	18.11	20.1		—	
9	51.61 - 52.70		—			—		(212) (130)	0.77	2.2	(340) (332)	24.65	28.6	(022)	34.58	34.8
10	52.71 - 53.80		—			—		(311) (122)	18.31	27.5	(150) (133)	2.27	3.9		—	
11	53.81 - 55.40		—		(121) (003)	30.55	26.8		—		(341) (242) (151)	3.26	4.3		—	
RI_i[d]		1.0000			1.5443			1.3825			0.9235			1.7668		

[a] Aldrich analytical reagent.
[b] Average of several commercial preparations.
[c] Broken Hill Associated Smelters Pty. Ltd. "baghouse" lead.
[d] Defined in terms of the most intense reflection group for each phase [15, 16, 20].

either the DSC or the acetic acid method, this lead value was introduced into the diffraction data analysis program as an independent measurement. The weight percentages of the oxides (α-PbO, β-PbO and Pb_3O_4) were then determined from eqn. (1), using equal weights for all peaks measured from a given phase, and taking into account the sample weight corresponding to the lead particles encapsulated by oxides that were not detected by the XRD procedure. The accuracy of the determination of the abundance of a particular phase in a sample is difficult to estimate since it will depend on the intrinsic degree of preferred orientation, microabsorption, etc. However, multiple determinations carried out on the same samples by different operators suggest that the error is about 3 wt.%.

Any difference between the sum of the oxide and lead weight percentages and 100% was then considered to represent the amount of amorphous material in the sample. Analysis of the amorphous content is the least reliable of the phase determinations since any errors in the oxide and lead weight percentages can accumulate in this measurement; its reliability can only be inferred from the range of values obtained for a wide variety of samples. For example, the minimum and maximum amorphous material contents for any sample should be 0.0 wt.% and 100.0 wt.%, respectively, and samples giving intense, sharp diffraction patterns should be reasonably crystalline, with relatively low amorphous contents. In the phase analysis results reported below (Table 3), the minimum amount of amorphous material was observed to be −5.0 wt.% (Barton pot leady oxide, BP2), and the maximum amount was 41 wt.% (standard β-PbO). This range is acceptable; analysis of a large body of data indicates that the absolute error in the amorphous content is in the vicinity of ±7 wt.%.

In the absence of an independent determination for the free-lead content, the phase analysis program can estimate the abundance of this phase from the diffraction data itself, based on a series of calibration experiments that compensate for the effect of lead encapsulation. However, the values so obtained are less reliable than the DSC and the acetic acid measurements, especially for lead contents greater than about 30 wt.% (see Fig. 3(b), and Table 3 below).

Pore-size and surface-area measurements

Mercury porosimetry

Mercury intrusion porosimetry was used to determine the total specific pore volume, the cumulative and differential pore-size distributions (for both pore volume and pore surface area), and the bulk and skeletal densities.

The determination of both the size and the volume of pores with a mercury penetration method is based on the behaviour of non-wetting liquids in capillaries. When a liquid, such as mercury, makes a contact (wetting) angle with a solid that is more than 90°, an externally applied pressure is required to force the liquid into the capillaries that constitute the porosity of the solid. If each of these capillaries is assumed to be an

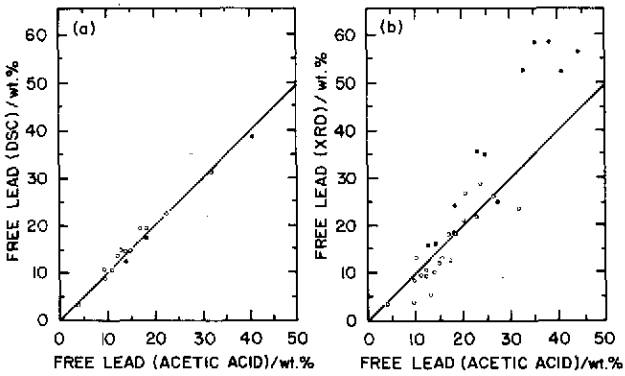

Fig. 3. Comparison between the free-lead content of various leady oxides measured by acetic acid dissolution and that determined by (a) DSC, and (b) XRD methods. The lines represent the 1:1 relationship between the two quantities; the filled and open circles represent leady oxides manufactured by the ball mill and Barton pot processes, respectively.

infinitely long cylinder that can be intruded by the liquid, then the diameter d of the cylinder is related to the applied pressure p by the relationship

$$d = -4\gamma \cos \theta / p \tag{3}$$

where γ is the surface tension of the liquid (*i.e.* mercury) and θ is the contact angle. Measurements of the volume of mercury intruded for a given weight of solid as a function of increasing pressure yield the cumulative, specific pore-volume plot as a function of decreasing pore diameter. Estimates of the abundances of pores of various sizes are obtained by plotting the pore-volume changes for small pore-diameter intervals against the pore diameter (*i.e.* the differential pore-size distribution is obtained).

The bulk density of the solid is derived from the amount of mercury surrounding the sample at the lowest pressure; 0.01 MPa (1.4 psia) in this work. If the total specific pore volume is taken into account, then a skeletal density is calculated that includes all pores of diameter greater than 0.003 μm; the latter value corresponds to the maximum pressure of the equipment available, 380 MPa (55 000 psia) in this work. The difference between this skeletal density and that obtained from XRD data gives a measure of the volume of the inaccessible pores and those with diameters less than 0.003 μm.

Finally, the specific pore surface area can be determined from the pV work expended in forcing mercury into the pores, that is, from the work required to cover the pore surface area A. The latter is given by the integral

$$A = -(1/\gamma \cos \theta) \int_{V_{min}}^{V_{max}} p \, dV \tag{4}$$

where V_{min} and V_{max} are the intruded mercury volumes for maximum- and minimum-size pores, respectively. Sufficiently small volume increments are assumed by sampling at closely spaced pressure values.

The properties described above were examined for leady oxides using a Micromeritics Model 9200 mercury porosimeter at pressures in the range 0.01 - 380 MPa (*i.e.* pore-diameter range 125 - 0.003 μm).

Since other mercury porosimetry investigations conducted in our laboratories on formed negative-plate material have shown that the mercury in the glass cup of the penetrometer becomes very viscous and wets the surfaces of both the cup and the material under study, suggesting amalgamation with the lead phase in the material, we expected parallel studies on leady oxides to result in a similar amalgamation of the lead particles contained therein. However, after each run, the mercury had a low viscosity and a high contact angle, thus indicating that there was no significant amalgamation of the lead particles in the oxide. It is probable that in the case of leady oxides the lead particles are protected from amalgamation by an oxide coating formed during manufacture or by aging (see below).

BET surface area

The surface areas of both the internal pores and the external surface of solids are best determined by the physical adsorption of gases or vapours. The amount of gas adsorbed by a solid is obtained from a comparison of the equilibrium pressures in a closed system of constant volume when empty and when containing the solid sample. These data are used to calculate the volume of gas required to cover the surface with a monolayer of gas and, in turn, the total surface area is determined using an assumed value for the area covered by a molecule (or atom) of the adsorbate gas. The calculations are based on the assumption that for solids with pores of diameter greater than 20 Å, at least five to seven layers of gas will be adsorbed before condensation occurs. Brunauer *et al.* [23] showed that the volume V of gas adsorbed at an equilibrium pressure p is related to the monolayer volume V_0 by the relationship (known as the BET equation)

$$\frac{V}{V_0} = \frac{Cp/p_0}{(1-p/p_0)[1+(C-1)p/p_0]} \tag{5}$$

where p_0 is the saturation pressure of adsorbate gas at the temperature of the experiment, and C is a constant related to the heat of adsorption and must have a value greater than about 5.

Recasting eqn. (5) into linear form gives

$$\frac{p}{V(p_0-p)} = \frac{C-1}{V_0C}\frac{p}{p_0} + \frac{1}{V_0C} \tag{6}$$

from which $V_0 = 1/(\text{slope} + \text{intercept})$ for a linear regression line corresponding to points in the range $0.05 < p/p_0 < 0.35$.

The surface areas of the leady oxides reported here were obtained using krypton adsorption at the temperature of liquid nitrogen. Krypton was selected as the adsorbate gas because the oxides have a low surface area and therefore require a gas for which small quantities would result in a saturated vapour at the experimental temperature (350 Pa at −195 °C for Kr). The

samples were outgassed at 150 °C overnight, or until the pressure was less than 1.3 mPa. The adsorption measurements were carried out on a Carlo Erba Model 1820 instrument modified locally for automated operation with krypton.

Results and discussion

Analysis of "standard" leady oxide components

Table 2 contains a list of the intensities of the scanned peaks for representative samples of commercial "standard" lead, α-PbO, β-PbO and Pb_3O_4. For all samples, the integrated observed peak intensities for each scan region agree reasonably well with the calculated values, although there is clearly some degree of residual preferred orientation manifest in certain peak intensities (*e.g.* the pair of peaks 311 and 122 for β-PbO). This is not surprising since both α-PbO and β-PbO have a pronounced layering in their structures and crystallize with a plate-like habit. As indicated above, an attempt has been made in the analytical procedure to minimize this preferred orientation by measuring the intensity of three peaks from both of these phases.

The phase analysis results given in Table 3 for the above standard materials (α-PbO, β-PbO and Pb_3O_4) confirm that commercially manufactured samples are not always completely phase-pure, especially if the samples have been stored for long periods of time in uncontrolled conditions. Furthermore, some of the samples are very poorly crystalline, containing up to 41% of their mass as amorphous material (*e.g.* β-PbO). Similar levels of non-crystalline material have been observed previously in many samples of lead dioxide (both α-PbO_2 and β-PbO_2) prepared both by chemical and by electrochemical methods [18, 21, 22, 24 - 28]. These results underline the importance of using calculated, rather than observed, reference intensity ratios in the fundamental phase-concentration/peak-intensity relationship (eqn. (1)). Otherwise, the "hidden" amount of amorphous material contained in the standard oxides used for experimental calibration would be propagated through all of the subsequent analyses of oxides of unknown composition.

Analysis of leady oxides

A total of 34 commercially prepared leady oxides from four continents has been received as part of our continuing studies of oxide characteristics and their effect on paste and plate manufacture and subsequent cycling performance in batteries subjected to deep-discharge service. Ten of these samples were produced by the ball mill process, and the remaining 24 samples by the Barton pot method (Table 3). All but two of the samples (BM5 and BP11 in Table 3) were produced during "normal" operation of the manufacturing process. Most of the oxides have been characterized by all three of the analytical methods outlined above; many have been

photographed with an optical microscope for qualitative determination of particle size, phase relationships, and morphology; and some have been subjected to quantitative particle-size and surface-area measurements. In the following discussion, we shall concentrate on those oxides that could be analysed very soon (*i.e.* less than a week) after production (termed "fresh" oxides). The oxides for which there was a longer delay between manufacture and analysis (mostly due to transport delays) display broadly similar properties to fresh samples made by the same process, but they have phase compositions that have altered systematically as a function of storage time (see below). These latter samples are termed "aged" and will be discussed in a later section on the effects of oxide storage.

Phase analysis determinations of both fresh and aged samples are summarized in Table 3. Oxides produced by the ball mill process have been separated from those produced by the Barton pot method. Ball mill oxides can be distinguished from those made by the Barton pot process (ignoring exotic samples BM5 and BP11) by:

(1) a slightly lower content of crystalline α-PbO (36 → 61 wt.%, mean 48.0 wt.% *versus* 37 → 70 wt.%, mean 52.8 wt.%);
(2) a much lower crystalline β-PbO content (0 → 4 wt.% *versus* 4 → 28 wt.%);
(3) a greater content of free lead (23 → 41 wt.% *versus* 10 → 32 wt.%);
(4) a slight tendency to have a higher content of amorphous material (8 → 21 wt.%, mean 14.8 wt.% *versus* 0 → 19 wt.%, mean 9.6 wt.%).

Thus, the conversion of lead to crystalline oxide (α-PbO + β-PbO + Pb_3O_4) is lower for the ball mill process (40 - 60 wt.%) than for the Barton pot process (65 - 95 wt.%). The concentration range of Pb_3O_4 remains constant for the two processes, but at a very low level ($\leqslant$ 3 wt.%).

The higher amorphous content of the ball mill oxides is in agreement with the empirical observation (Table 1) that the milling procedure gives a higher proportion of small particles. The uniformly low crystalline β-PbO content of the ball mill oxides is consistent with the expected preferential formation of the low-temperature polymorph, α-PbO, at the lower operating temperature of the ball mill relative to the Barton pot process. The Barton pot oxides do, however, display a wide range of β-PbO contents (4 - 28 wt.%, with an upper value of 77 wt.% if sample BP11 is taken into account), and thereby suggest that the operating parameters of the different Barton pots can vary considerably between manufacturers. Since it is generally held [7] that the concentration of β-PbO should be below about 15 wt.% for satisfactory plate performance, it is clear that some of the Barton pots are operated under less than optimum conditions.

In order to test the variability in the composition of ball mill leady oxide during a specific production run, samples were obtained from a manufacturer both at start-up and at mid-run of the mill. Phase analysis showed that at mid-run the oxide (BM2 in Table 3) had an α-PbO content higher by 19.6 wt.%, a free-lead content lower by 11.5 wt.%, and an amorphous content lower by 8.7 wt.% than that in the oxide at start-up (BM5).

TABLE 3

Summary of DSC, acetic acid and XRD phase analysis results (wt.%), and other properties, of oxide standards and various commercial leady oxides

Oxide	α-PbO	β-PbO	Free Pb[b]			Pb_3O_4	Amorphous	α-PbO:β-PbO ratio	Colour
			DSC	HAc	XRD				
Standard									
α-PbO	64.8	8.1	0.0	—	1.2	7.6	19.5	8.0	—
β-PbO	1.3	52.2	0.0	—	2.0	5.9	40.8	0.03	—
Pb_3O_4	0.0	2.8	0.0	—	0.0	81.1	16.2	0.0	—
Ball mill (fresh)									
BM1	60.5	2.5	—	24.7	34.9	3.1	9.2	24.2	Green
BM2 (mid-run)	54.8	4.0	—	32.5	58.1	0.7	8.0	13.7	Grey
BM3	53.0	2.0	—	23.0	35.6	3.3	18.7	26.5	Green
BM4	36.8	0.5	38.6	40.5	52.1	2.7	21.4	73.6	Green
BM5 (start-up)	35.2	3.3	—	44.0	56.2	0.7	16.7	10.7	Grey
Range[a]	36 - 61	0 - 4		23 - 41		0 - 3	8 - 21	14 - 74	
Ball mill (aged)									
BM1	70.5	3.2	—	18.2	25.7	2.2	5.8	22.0	Green
BM3	64.3	2.7	17.3	18.2	24.0	2.2	13.6	23.8	Green
BM6	61.3	3.8	—	12.5	15.8	1.4	21.0	16.1	Brown
BM7	60.6	3.5	12.3	14.1	15.9	6.2	17.6	17.3	Brown
BM4	50.2	3.0	—	34.0	44.8	0.8	11.9	16.7	Green
BM8	43.3	7.1	—	32.5	52.6	6.8	10.3	6.1	Green
BM9	41.7	2.1	—	27.2	24.9	2.6	26.5	19.9	Brown
BM10	38.8	6.5	—	37.0	58.3	4.4	13.2	6.0	Green
Range	38 - 71	2 - 7		14 - 37		0 - 7	6 - 27	6 - 24	
Barton pot (fresh)									
BP1	70.2	8.8	—	12.3	10.7	0.9	7.8	8.0	Red
BP2	67.2	24.8	—	10.1	13.2	3.0	−5.0	2.7	Brown

BP3	67.2	4.3	—	23.6	28.7	1.8	3.1	15.6	Red
BP4	61.9	12.2	—	20.3	26.6	1.9	3.7	5.1	Brown
BP5	53.8	6.4	21.2	—	17.5	0.0	18.7	8.4	Red
BP6	47.4	8.9	—	26.3	26.1	1.7	15.7	5.3	Brown
BP7	44.3	23.2	—	15.6	13.1	1.3	15.6	1.9	Red
BP8	39.7	18.8	—	31.5	34.2	1.3	8.8	2.1	Red
BP9	38.0	27.8	—	20.0	21.2	1.6	12.5	1.4	Brown
BP10	37.8	27.5	19.4	16.9	18.0	0.0	15.3	1.4	Red
BP11	5.3	77.2	10.8	9.5	3.9	0.8	7.2	0.1	Green
Range[a]	37 - 70	4 - 28		10 - 32		0 - 3	0 - 19	1 - 16	
Barton pot (aged)									
BP5	88.3	7.1	—	5.5	6.9	0.2	−1.1	12.4	Red
BP4	75.8	13.7	—	6.9	7.7	0.8	2.8	5.5	Brown
BP12	72.2	4.6	14.7	13.1	5.5	1.8	6.7	15.7	Red
BP13	71.5	4.8	3.3	4.0	3.6	4.4	16.0	14.9	Very red
BP14	68.5	6.9	9.0	9.7	8.5	3.5	12.2	9.9	Red
BP15	65.8	4.5	14.9	15.0	12.0	2.0	12.8	14.6	Red
BP16	64.3	3.4	14.4	14.0	10.1	3.6	14.3	18.9	Red
BP6	63.7	8.3	—	15.3	11.4	1.4	11.4	7.7	Brown
BP17	63.6	9.1	10.7	11.1	9.6	2.0	14.7	7.0	Red
BP18	59.5	6.9	—	17.9	18.2	2.1	13.6	8.6	Brown
BP9	56.0	26.9	—	5.3	4.5	2.0	9.8	2.1	Brown
BP19	55.0	18.8	13.7	12.3	9.4	4.1	8.4	2.9	Red
BP20	54.0	17.1	19.3	18.3	18.2	2.4	7.2	3.2	Brown
BP21	53.3	3.2	22.7	22.8	21.8	4.4	16.4	16.7	Red
BP22	43.4	3.5	31.0	31.6	23.4	1.1	21.1	12.4	Brown
BP23	37.1	24.0	—	17.3	12.7	2.2	19.4	1.6	Brown
BP24	34.5	40.0	13.3	—	28.3	0.3	12.1	0.9	Red
BP11	5.7	80.7	—	9.4	4.6	0.5	3.6	0.1	Green
Range[a]	34 - 88	3 - 40		4 - 32		0 - 4	2 - 21	1 - 19	

[a] Ignoring oxide BM5 or BP11.

[b] Free-lead content determined by differential scanning calorimetry (DSC), acetic acid dissolution (HAc), or X-ray diffraction (XRD).

These differences are almost as large as those obtained between samples from different manufacturers. If uniformity in the oxide composition for a particular pasting batch is desired, then these results suggest that urgent attention should be given to the variations in process parameters both within and between leady oxide production runs.

The amount of amorphous material in all (*i.e.* fresh and aged ball mill and Barton pot) oxides examined so far is less than 27 wt.%. However, other studies performed in our laboratories indicate that the amount of this component rises to values above 40 wt.% after curing [29].

Aging of leady oxides during storage

The composition of leady oxides can change during storage at room temperature owing to the continued oxidation of the particles of free lead. Since these oxides may be held over in the factory between plate-pasting runs, it is possible that the change in oxide characteristics during the intervening time could significantly alter the performance of the final battery plate product. We have, therefore, endeavoured to measure quantitatively the rate and extent of these compositional modifications, and to determine the identity of the oxidation product, for samples of both Barton pot and ball mill oxides. The experimental programme involved both one-shot and periodic phase analysis of samples stored at low temperature (2 °C) and at room temperature (~ 23 °C). The results are summarized in Table 4 and in Fig. 4.

The data show that the free-lead content remained reasonably stable when the oxides were kept at reduced temperature. At room temperature, the major effects of storage are broadly similar for ball mill and Barton pot oxides, namely:

(1) a significant decline in the free-lead content, *e.g.* 20 wt.% to 7 wt.% over a period of two months for BP4 (Table 4);

(2) a correspondingly large increase in the α-PbO content, *e.g.* 62 wt.% to 76 wt.% for BP4;

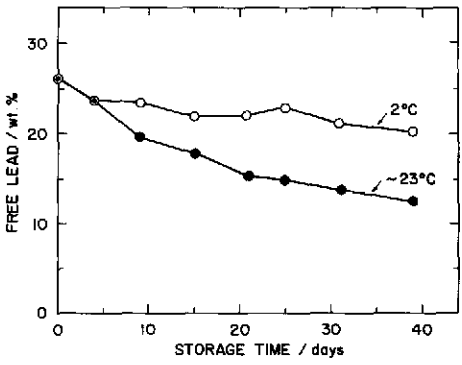

Fig. 4. Free-lead content (acetic acid) of samples of ball mill leady oxide as a function of storage time at 2 °C and room temperature (~ 23 °C).

TABLE 4

Phase analysis results for leady oxides in the fresh and aged condition

Oxide		Age (days)	α-PbO	β-PbO	Free Pb (HAc)	Pb_3O_4	Amorphous	α-PbO:β-PbO ratio
Ball mill								
BM1	Fresh	0	60.5	2.5	24.7	3.1	9.2	24.2
	Aged (2 °C)	35	70.1	3.8	23.3	1.2	1.2	18.4
	Aged	35	70.5	3.2	18.2	2.2	5.8	22.0
BM3	Fresh	0	53.0	2.0	23.0	3.3	18.7	26.5
	Aged	17	64.3	2.7	18.2	2.2	13.6	23.8
BM4	Fresh	0	36.8	0.5	40.5	2.7	21.4	73.6
	Aged (2 °C)	28	53.6	3.4	35.4	1.7	5.9	15.8
	Aged	28	50.2	3.0	34.0	0.8	11.9	16.7
Barton pot								
BP4	Fresh	0	61.9	12.2	20.3	1.9	3.7	5.1
	Aged	63	75.8	13.7	6.9	0.8	2.8	5.5
BP5	Fresh	0	53.8	6.4	21.2	0.0	18.7	8.4
	Aged	360	88.3	7.1	5.5	0.2	−1.1	12.4
BP6	Fresh	0	47.4	8.9	26.3	1.7	15.7	5.3
	Aged	140	63.7	8.3	15.3	1.4	11.4	7.7
BP9	Fresh	0	38.0	27.8	20.0	1.6	12.5	1.37
	Aged	140	56.0	26.9	5.3	2.0	9.8	2.08
BP11	Fresh	0	5.3	77.2	9.5	0.8	7.2	0.07
	Aged (2 °C)	20	7.4	79.8	9.8	0.0	3.0	0.09
	Aged	20	5.7	80.7	9.4	0.5	3.6	0.07

Except where otherwise indicated, all analyses were determined on oxides stored at about 23 °C.

(3) a relatively small (absolute) increase in the β-PbO content (leading, in the case of ball mill oxides, to an overall decrease in the ratio of α-PbO to β-PbO);

(4) a decrease in the amount of amorphous material.

It was expected that the lead would oxidize predominantly to the low-temperature polymorph, α-PbO, but the decrease in amorphous material was not anticipated. We note that, whereas the changes in free-lead content are mainly dependent upon temperature, the conversion of amorphous material to crystalline product (predominantly α-PbO) is also dependent upon the time interval of storage (*e.g.* 61 → 70 wt.% α-PbO for BM1 stored at 2 °C for 1 month). On the other hand, inspection of the surface-area and pore-size distribution data (see Table 5 and discussion below) does not indicate any trend in the pore-structure properties with sample age or storage temperature.

In Fig. 4, the change in the free-lead content (acetic acid method) of two samples of the same ball mill oxide has been plotted as a function of storage time. One sample was stored at room temperature (~ 23 °C), the other was kept at 2 °C. The data clearly demonstrate that at room temperature, the free-lead content decreases at a relatively constant rate of about 0.5 wt.% per day for the first three weeks of storage, whereupon the rate declines to less than 0.2 wt.% per day for the remaining period of storage (about three weeks). On the other hand, the sample kept at 2 °C shows a decline in free-lead content of only about 0.15 wt.% per day over the entire storage period (about six weeks). Similar calculations performed on Barton pot oxides show that, in general, the rate of free-lead conversion appears to be somewhat lower for Barton pot oxides than for ball mill oxides (Table 4), indicating that the shelf-life is longer for the former material (as noted in Table 1).

As yet, we have not studied the effect of compositional and morphological changes of leady oxide on the performance of cured and formed plates manufactured from the oxide. Industry generally accepts that the initial free-lead content of the oxide should be in the range 15 - 25 wt.%. The above studies indicate that when an oxide is manufactured with a free-lead content slightly above or near the upper limit of this range, the oxide can be stored for lengthy periods under cool conditions. On the other hand, it is possible that an oxide with an initially low free-lead content may become unsuitable for use in paste-making if it is not utilized soon after production.

Optical microscopic examination of leady oxide morphology

Visual observation of spatial relationships between the component phases in leady oxides (or indeed any complex mixture of compounds) is of particular importance in attempts to rationalize measurements of their surface area, particle and pore-size distribution, and chemical and/or electrochemical reactivity. The general trend in recent years has been to use scanning electron microscopy (SEM) for studies of this kind since this

technique allows very high magnifications to be achieved simultaneously with a good focal depth-of-field. However, SEM equipment is expensive (and therefore is not generally available to infrequent users such as battery manufacturers), requires extensive training for its operation, and produces sample images only in shades of grey. On the other hand, examination of leady oxides under a high-quality optical microscope has many advantages: the equipment is relatively inexpensive and easy to operate, sufficiently high magnifications can be achieved if polished mounts of the material are prepared, and the component phases can be readily distinguished on the basis of their different colours.

Leady oxide powder was prepared for optical examination by mixing a small quantity of the oxide with epoxy resin, mounting this in a cavity in a carbon-impregnated epoxy block, allowing it to set, and then polishing the surface with 600 grade silicon carbide paper followed by successive polishing with 6, 3 and 1 μm diamond pastes. The polished mounts were then examined under normal-incidence polarized white light in a Reichert optical microscope at magnifications of 180X, 350X and 1800X. Colour photographs were taken of areas of particular interest.

Figure 5(a) is an optical micrograph of a fresh U.K. ball mill leady oxide sample 1 (BM3 in Table 3). The light brown, elongated or flaky, particles are free lead (23 wt.%), and the yellow/green regions are either α-PbO (53 wt.%) or β-PbO (2 wt.%); the small amount of Pb_3O_4 present in this sample (3 wt.%) cannot be distinguished at this magnification. A corresponding micrograph of a fresh Australian Barton pot leady oxide sample 1 (BP8 in Table 3, Fig. 5(b)) is quite different in appearance. In this oxide, the dark-brown lead particles (32 wt.%) are roughly equidimensional in shape, the individual particles of yellow/green α-PbO (40 wt.%) and β-PbO (19 wt.%) can just be discerned, and a single large particle of orange Pb_3O_4 (1 wt.%) is visible in the upper-middle portion of the micrograph.

Optical micrographs of other U.K. manufacturers' fresh ball mill oxide sample 2 (BM4; 41 wt.% free lead) and Barton pot oxide sample 2 (BP5; 21 wt.% free lead) are given in Figs. 5(c) and (d), respectively. The same characteristics are observed, namely, the ball mill oxide has elongated lead particles and PbO particles of sub-microscopic size, whereas the Barton pot oxide has equidimensional lead particles and larger PbO particles. These results are consistent with the higher amorphous content and smaller mean particle size observed for ball mill oxides relative to Barton pot varieties (see Table 3 and discussion below).

It is, however, only when the oxides in Figs. 5(c) and (d) are examined under high magnification (Figs. 5(e) and (f)) that the detailed spatial relationships between the lead and oxide particles become clear. The individual PbO particles in the ball mill oxide are still barely visible, but the PbO particles in the Barton pot oxide are shown to be well separated, roughly spherical, and of fairly uniform size. The background colour of the PbO in the two types of oxide is also quite different. Since both oxides contain only about 2 wt.% Pb_3O_4, the Barton pot oxide appears redder in colour

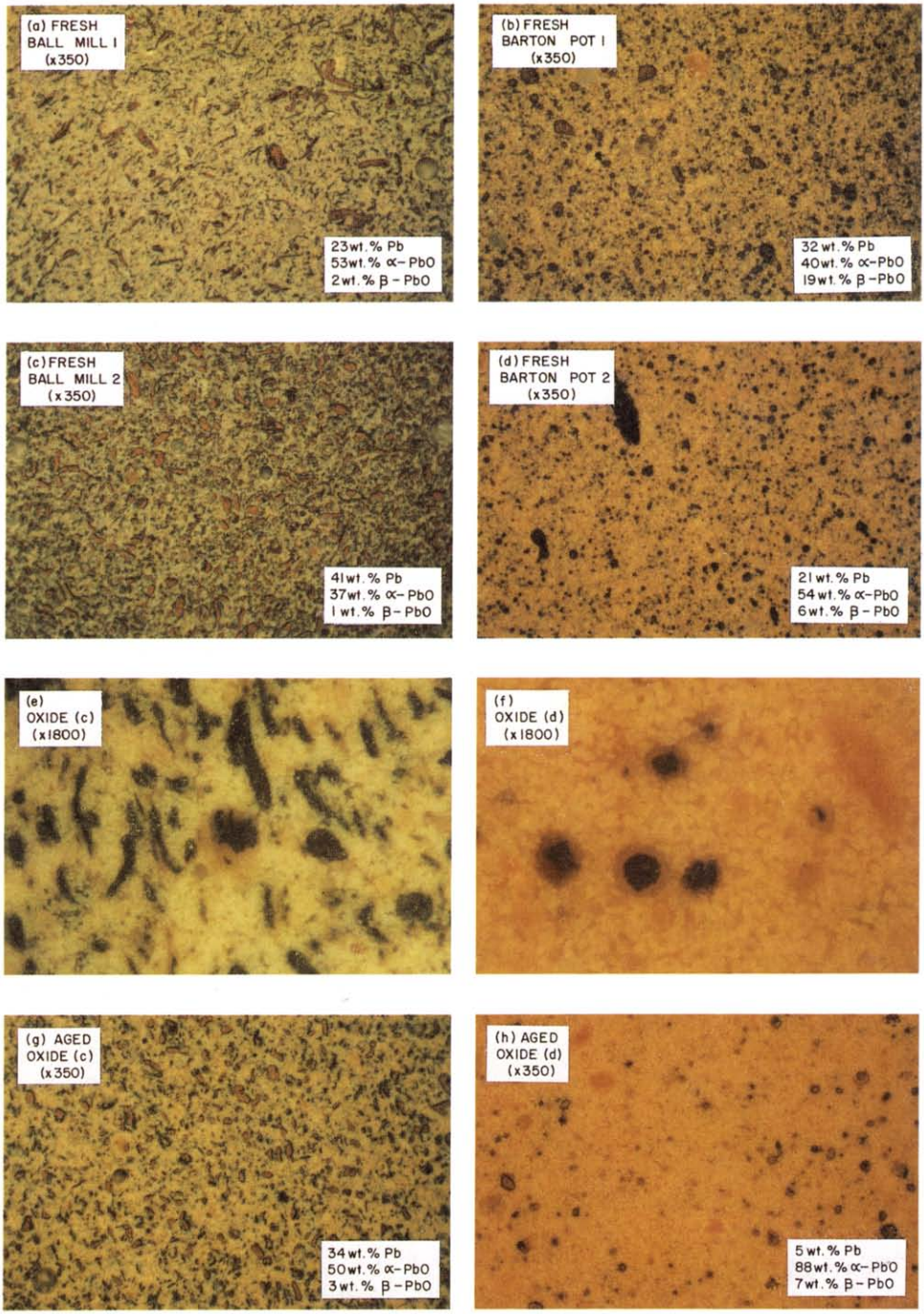

Fig. 5. Optical micrographs of polished mounts of leady oxide samples. (Reduced in reproduction $\times\frac{1}{2}$.)

probably because of its higher α-PbO content (54 wt.% relative to 37 wt.%) and its lower content of free lead (21 wt.% relative to 41 wt.%). We note that, in general, the ball mill oxides are green/grey in colour and the Barton pot oxides are red/brown (Table 3). This colour difference occurs over a wide range of α-PbO to β-PbO ratios and it is clear that the dominant factor in determining oxide coloration is the content of free lead: oxides containing large amounts of free lead tend to be grey/green, while those with smaller amounts are red/brown.

The two micrographs in Figs. 5(e) and (f) clearly demonstrate the large difference in free-lead content of the two oxides under study, *i.e.* 41 wt.% *versus* 21 wt.% free lead for ball mill oxide *versus* Barton pot oxide. The lead particles in both oxides show a large variation in size and are, in some cases, surrounded by quite thick reaction rims of oxide. This encapsulation of the lead particles, together with their size variability (and, therefore, chemical reactivity), demonstrates why X-ray diffraction and wet-chemical methods of free-lead determination, unless carefully controlled, are unlikely to provide accurate estimates of the amount of unreacted lead. This also applies to wet-chemical analytical techniques that do not specifically provide for the presence of the "mixed" oxide Pb_3O_4, containing lead in the 2^+ and 4^+ oxidation states.

Figures 5(g) and (h) are low-magnification micrographs of the two leady oxides shown in Figs. 5(c) and (d), respectively, after storage at room temperature for extended periods (28 days and 360 days, respectively). The decline in free-lead content of the ball mill oxide from 41 wt.% to 34 wt.% (*cf.* Figs. 5(c) and (g)), and of the Barton pot oxide from 21 wt.% to 5 wt.% (*cf.* Figs. 5(d) and (h)) is clearly visible, particularly with respect to the remaining number of very small particles of lead.

Pore-size distribution and surface area of leady oxides

The results of pore and surface studies on the oxides are summarized in Table 5 and Fig. 6. The cumulative pore volumes for ball mill oxides

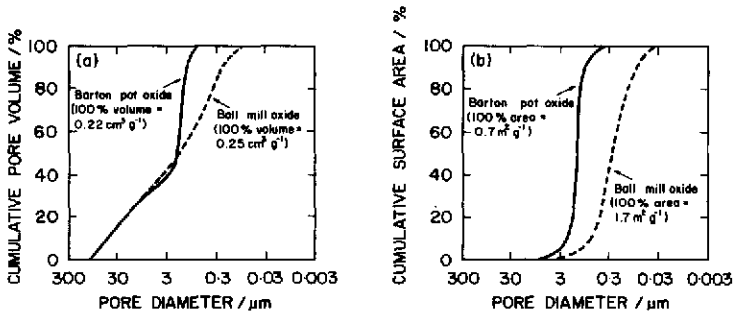

Fig. 6. Comparison of (a) cumulative pore volume and (b) surface area of typical ball mill and Barton pot leady oxides. The volumes and areas are expressed as percentages of the total values and are plotted as a function of the pore diameter on a logarithmic scale.

TABLE 5

Surface-area, porosity and density data for leady oxides

Oxide	Total pore volume[c] ($cm^3\ g^{-1}$)	Bulk density[c] ($g\ cm^{-3}$)	Skeletal density[c] ($g\ cm^{-3}$)	SSA[a] porosimetry[c] ($m^2\ g^{-1}$)	SSA BET (Kr)[c] ($m^2\ g^{-1}$)	Median pore diam.[c] (μm)	Modal pore diam. (μm)	Cumulative pore-volume distribution over stated pore-diameter range[b]	
Standard								Broad from	Narrow from
α-PbO	0.332	2.10	7.00	0.56	0.30	3.23	2.8	75 to 3	3 to 1.1
β-PbO	0.159	3.62	8.48	0.27	0.31	2.31	0.5	90 to 6	6 to 0.3
Ball mill								Overlapping broad pair from	
BM4 (fresh)	0.213	2.67	6.20	1.52	1.79(1)	1.71	0.23	60 to 0.13	
BM3	0.298	2.04	5.21	2.42	1.77	2.67	0.18	90 to 0.15	
BM7	0.248	2.62	7.50	1.69	1.73(1)	1.67	0.25	70 to 0.15	
BM9	0.20(5)	3.1(5)	7.78(22)	1.24(9)	1.16(1)	2.23(12)	0.35	80 to 0.2	
Barton pot								Broad from	Narrow from
BP3 (fresh)	0.218	2.91	7.92	0.76	0.84	1.50	1.2	70 to 1.7	1.7 to 0.3
BP7 (fresh)	0.192(27)	2.90(5)	6.8(14)	0.46(3)	0.64(1)	2.64(8)	2.4	80 to 2.5	2.3 to 0.8
BP12	0.264	2.56	7.84	0.73	0.82(5)	1.76	1.3	70 to 1.8	1.8 to 0.4
BP13	0.264(20)	2.30(9)	6.0(7)	0.77(2)	0.82(2)	1.62(8)	1.2	80 to 1.5	1.5 to 0.5
BP22	0.211	2.93	7.72	0.51	0.55	2.37	1.8	75 to 2.4	2.4 to 0.7
BP24	0.198	2.93	6.96	0.35	0.65(1)	1.87	1.4	70 to 2.0	2.0 to 1.1

[a]SSA = specific surface area.

[b]Pore diameters given in μm; range extremes correspond to 5 and 95% of the total pore volume.

[c]Numbers in parentheses represent the estimated error (from multiple determinations) in the least significant figure to the left.

when plotted (not shown here) as normal probabilities *versus* ln d are indicative of two broad overlapping normal distributions. Over 95% of the total pore volume is accounted for by pores with diameters in the range 90 - 0.13 μm. On the other hand, analogous normal probability plots of data for Barton pot oxides show the existence of two differently shaped normal distributions of pores: the one in the 80 - 1.5 μm pore-diameter range, which accounts for 40% of the total pore volume, is identical in shape to that of ball mill oxides; while the other between 2.4 and 0.3 μm has a much narrower spread. This is manifest on the cumulative plot as a sharp rise over a narrow pore-diameter range (Fig. 6(a)). Indeed, 45% of the total pore volume is contained within this narrow distribution of pores. Similar observations obtained in an earlier study [30] were attributed to the lower content of β-PbO in the oxides made by the ball mill process, leading to a higher BET specific surface area and a higher discharge capacity of plates made from this oxide.

The differential pore-volume distributions show (Table 5) that the most frequent (modal) pore diameter for ball mill oxides is typically ~0.2 μm, whereas for Barton pot oxides the value is ~1.5 μm. It is not surprising, therefore, that surface areas for ball mill oxides are significantly greater than those for their Barton pot counterparts, namely 1.7 $m^2\ g^{-1}$ *versus* 0.7 $m^2\ g^{-1}$ (Fig. 6(b)). It will be seen from Table 5 that the specific surface areas derived from porosimetry are, at best, in qualitative agreement with the much more reliable BET data.

It is noted (Table 5) that the skeletal densities of leady oxide samples from both processes are low (average 7.3 g cm^{-3}) compared with the XRD-derived individual densities of PbO, Pb_3O_4 and Pb (9.5, 9.1 and 11.35 g cm^{-3}, respectively). This implies particle porosities of ~20%; these could be either due to inaccessible pores with diameters greater than about 0.003 μm, or to micropores for which there is no evidence from either porosimetry or gas adsorption. Indeed, recent measurements of the bulk hydrogen content of formed positive-plate material [28, 31, 32] suggest that significant quantities of hydrogen (as adsorbed hydroxyl groups) reside on "internal" particle surfaces and/or in trapped pores that remain inaccessible to surface-area measurements. It is also possible that a correlation exists between the low skeletal densities and the amorphous content of the oxide, and this aspect will be examined further.

Conclusions

A full quantitative analysis of the phases present in commercial leady oxides used in battery plate manufacture requires a combination of careful X-ray diffraction measurements with an independent determination of the free-lead content. This is because some particles of lead are only partially oxidized during the ball mill or Barton pot process and are therefore encapsulated by the lead oxide phases so produced. In the present study,

the phase analysis is accomplished by the development of an XRD technique that utilizes CeO_2 as an internal standard, and takes the free-lead content obtained either by measuring the enthalpy of melting of lead by differential scanning calorimetry, or by dissolving away the oxides in a development of the well-known acetic acid method. The X-ray reference intensity ratios and relative peak intensities of all of the component phases are determined by calculation from the crystal structure parameters, rather than by measurement experimentally. This procedure minimizes problems normally encountered with the phase purity, preferred orientation and crystallinity of standard samples used for calibration.

The phase analysis results have revealed significant differences between the chemical compositions of ball mill and Barton pot leady oxides. In general, fresh ball mill material contains significantly less (crystalline) β-PbO than Barton pot material. The preferential formation of β-PbO in the Barton pot is expected since this is the high-temperature polymorph and the Barton pot process operates at high temperatures. The α-PbO and Pb_3O_4 contents of both types of oxide are about the same, with the latter oxide being present in only minor amounts. Overall, the rate of conversion of lead to crystalline lead oxides is lower for the ball mill process. This is reflected by greater proportions of amorphous material and free lead in this type of oxide.

A significant observation is that there can arise marked differences in the composition of Barton pot oxide, particularly as regards the proportion of β-PbO. Several samples of Barton pot oxide were found to contain β-PbO contents at a level considered detrimental to plate performance. In these cases, the suitability of the process variables in operation at the time of production of these oxides is open to question. Furthermore, both Barton pot and ball mill oxides show large variations in free-lead content within and between production runs. Storage of the leady oxide at room temperature can result in significant conversion of the free lead and amorphous material to PbO (predominantly the α-PbO polymorph). Oxide stability appears to be higher for Barton pot than for ball mill oxides (independent of the free-lead content), and can be improved for both oxide types by storage under cool conditions.

Mercury porosimetry and gas adsorption measurements allow ball mill and Barton pot oxides to be readily distinguished by virtue of their individual characteristic pore-size distributions and markedly different surface areas. The most obvious differences between the two types of oxides are, firstly, that ball mill oxides have pores forming two overlapping distributions whereas Barton pot oxides have one broad distribution and one of narrow spread, and secondly, that the specific surface areas of ball mill oxides are significantly higher than those of Barton pot oxides.

Traditionally, the lead/acid battery industry has accepted that the physico-chemical characteristics of leady oxide exert little influence on battery performance after a short period of service. The study reported here has revealed that marked changes in leady oxide chemistry and morphology

can occur with different production methods, during the same production run, or on storage of the oxide. Such changes question batteryman's lore. We suggest that differences in the nature of the leady oxide could produce a significant effect on the eventual electrochemical, chemical and mechanical properties of battery plates. Experiments are currently in progress in our laboratories to test this proposal. Should our findings show that there is indeed a dependence of battery behaviour on leady oxide properties, then the vital question that remains to be answered is whether there is an optimum oxide composition and/or morphology conducive to good performance in each of the different applications of the lead/acid battery.

Acknowledgements

The authors are indebted to their colleagues W. G. A. Baldsing and K. Constanti for assistance with the X-ray determinations, to D. C. Constable for help with the optical microscopy, and to T. Lwin for useful discussions on numerical distributions. We thank the Australian Associated Smelters Pty. Ltd. for financial assistance and for permission to publish the results of this study.

References

1 A Special Issue Devoted to Lead–Acid Batteries, D. H. Collins (ed.), *J. Power Sources, 2* (1977) 39.
2 N. E. Hehner, *Storage Battery Manufacturing Manual II*, Independent Battery Manufacturers Assoc. Inc., Largo, FL, 1981, p. 17.
3 N. E. Hehner, in *Lead Oxides: Chemistry, Technology, Battery Manufacturing Uses, History*, Independent Battery Manufacturers Assoc. Inc., Largo, FL, 1974, pp. 5 - 12.
4 T. Blair, in *Improvements in Alloys, Oxides and Expanders for Lead Acid Batteries*, Lead Development Assoc., London, 1984, pp. 8 - 14.
5 J. R. Dafler, *J. Electrochem. Soc., 124* (1977) 1312.
6 V. Iliev and D. Pavlov, *J. Appl. Electrochem., 9* (1979) 555.
7 M. Barak, in M. Barak (ed.), *Electrochemical Power Sources: Primary and Secondary Batteries*, Peter Peregrinus, Stevenage, U.K., 1980, p. 223.
8 R. Stillman, R. Robins and M. Skyllas-Kazacos, *J. Power Sources, 13* (1984) 171.
9 A. De La Torre, M. Torralba, A. Garcia and P. Adeva, *J. Power Sources, 15* (1985) 77.
10 R. T. Morano, *Thermochim. Acta, 26* (1978) 27.
11 R. Hultgren, P. D. Desai, D. T. Hawkins, M. Gleiser, K. K. Kelly and D. D. Wagman, *Selected Values of the Thermodynamic Properties of the Elements*, Am. Soc. Metals, Ohio, 1973.
12 H. Bode, *Lead–Acid Batteries*, Wiley, New York, 1977, p. 212.
13 M. Denby, in D. H. Collins (ed.), *Batteries*, MacMillan, New York, 1963, p. 440.
14 H. F. Steger, *Talanta, 23* (1976) 84.
15 K. Matsumoto and Z. Fresenius, *Anal. Chem., 305* (1981) 370.
16 H. P. Klug and L. E. Alexander, *X-ray Diffraction Procedures for Polycrystalline and Amorphous Materials*, Wiley, New York, 1954, p. 410.
17 D. Pavlov, V. Iliev, G. Papazov and E. Bashtavelova, *J. Electrochem. Soc., 121* (1974) 854.

18 R. J. Hill, Quantitative X-ray diffraction phase analysis and its application to the positive plate of the lead/acid battery, *Commun. MCC 387, May 1982*, CSIRO Division of Mineral Chemistry, Port Melbourne, Vic. 3207, Australia, 33 pp.
19 R. J. Hill, *J. Power Sources, 9* (1983) 55.
20 R. J. Hill, *J. Power Sources, 11* (1984) 19.
21 D. C. Constable, J. R. Gardner, J. A. Hamilton, K. Harris, R. J. Hill, D. A. J. Rand, S. Swan and L. B. Zalcman, *ILZRO Project No. LE-290, Prog. Rep. 6, Jan.–Jun. 1982*, Int. Lead Zinc Res. Org. Inc., 76 pp.
22 K. Harris, R. J. Hill and D. A. J. Rand, *J. Electrochem. Soc., 131* (1984) 474.
23 S. Brunauer, P. H. Emmett and E. Teller, *J. Am. Chem. Soc., 60* (1938) 309.
24 N. E. Bagshaw, R. L. Clark and B. Halliwell, *J. Appl. Chem., 16* (1966) 180.
25 D. Kordes, *Chem.-Ing.-Tech., 38* (1966) 638.
26 S. M. Caulder and A. C. Simon, *J. Electrochem. Soc., 121* (1974) 1546.
27 K. Weisener and P. Reinhardt, *Z. Phys. Chem., 256* (1975) 285.
28 P. R. Skidmore and R. R. Schwartz, *Analyst, 104* (1979) 952.
29 R. J. Hill and A. M. Jessel, A study of the structure, chemistry and electrochemistry of positive plates in lead/acid batteries; Australian Associated Smelters, Pty. Ltd. sponsored project, *Prog. Rep. 3, Jun. 1984 - Feb. 1985, Commun. MCC 623, Mar. 1985*, CSIRO Division of Mineral Chemistry, Port Melbourne, Vic. 3207, Australia, 42 pp.
30 E. Skoluda, J. Kwasnik, K. Nowak and J. Kranska, *Electrochim. Acta, 17* (1972) 1353.
31 R. J. Hill, A. M. Jessel and I. C. Madsen, in K. R. Bullock and D. Pavlov (eds.), *Proc. Symp. on Advances in Lead–Acid Batteries, New Orleans, 8 - 11 Oct. 1984*, Vol. 84-14, The Electrochem. Soc., Pennington, NJ, pp. 59 - 77.
32 R. J. Hill and M. R. Houchin, *Electrochim. Acta, 30* (1985) 559.